# Measurements of the cross sections of the $^{186}$W$(n,\gamma)^{187}$W, $^{182}$W$(n,p)^{182}$Ta, $^{154}$Gd$(n,2n)^{153}$Gd, and $^{160}$Gd$(n,2n)^{159}$Gd reactions at neutron energies of 5 to 17 MeV

Rajnikant Makwana,[1] S. Mukherjee,[1,*] P. Mishra,[1] H. Naik,[2] N. L. Singh,[1] M. Mehta,[3] K. Katovsky,[4] S. V. Suryanarayana,[5]
V. Vansola,[1] Y. Santhi Sheela,[6] M. Karkera,[6] R. Acharya,[2] and S. Khirwadkar[3]

[1]*Physics Department, Faculty of Science, The Maharaja Sayajirao University of Baroda, Vadodara 390002, India*
[2]*Radiochemistry Division, Bhabha Atomic Research Centre, Mumbai 400 085, India*
[3]*Divertor Division, Institute for Plasma Research, Gandhinagar 382 428, India*
[4]*Department of Electrical Power Engineering, Brno University of Technology, Brno, Czech Republic*
[5]*Nuclear Physics Division, Bhabha Atomic Research Centre, Mumbai 400 085, India*
[6]*Department of Statistics, Manipal University, Manipal 576 104, India*

The cross sections of the $^{186}$W$(n,\gamma)^{187}$W, $^{183}$W$(n,p)^{183}$Ta and $^{154}$Gd$(n,2n)^{153}$Gd, $^{160}$Gd$(n,2n)^{159}$Gd reactions were measured at the neutron energies $5.08 \pm 0.165$, $8.96 \pm 0.77$, $12.47 \pm 0.825$, and $16.63 \pm 0.95$ MeV. Standard neutron activation analysis technique and off-line $\gamma$ ray spectrometry were used for the measurement and analysis of the data. Measurements were done in the energy range where few or no measured data are available. The results from the present work are compared with the literature data based on the EXFOR compilation. The experimental results are supported by theoretical predictions using nuclear modular codes TALYS 1.8 and EMPIRE 3.2.2. The predictability of different one-dimensional models available in TALYS 1.8 and Levden models in EMPIRE 3.2.2 were tested. A detailed comparison of experimental results with theoretical model calculations is made.

## I. INTRODUCTION

Nuclear reaction cross section data are of prime importance for reactor technology. When the reactor is in operation, it produces neutrons that penetrate through several materials, such as fuel, structural, controlling, and shielding materials, etc. It is important to have nuclear reaction cross section data for all these materials, at all possible neutron energies [1], for the development of the reactor technology. There are numerous measured nuclear data available in the EXchange FORmat (EXFOR) library [2]. However, it is important to have more experimental nuclear data, measured with high accuracy in the energy range between thermal and 20 MeV for a number of reactor materials [2]. Tungsten (W) and gadolinium (Gd) are two such materials. W is selected as a diverter material for the upcoming fusion device–International Thermonuclear Experimental Reactor (ITER) [3]. In ITER the DT reaction generates 14.6 MeV neutrons, which are scattered from the surrounding materials, thus neutrons will have energies from thermal to 14.6 MeV [4–9]. These neutrons interact with the diverter material of the reactor and can open different nuclear reaction channels. In accelerator driven subcritical system (ADSs), W is used in different parts, hence it can face neutrons with higher energies [10]. Further, Gd is an important rare earth element, which is used in control rods. Its nitrate form is useful for reactor control through moderator as liquid poison, as well as a secondary shutdown device in PHWR reactors [11]. Gadolinium nitrate is more advantageous due to its properties, such as high thermal neutron capture cross section, quick burnout, greater solubility, and a more efficient removal by ion exchange systems compared with

boron [12]. Hence it is important to have accurate cross section data for all the tungsten and gadolinium isotopes in the energy range from thermal to 20 MeV. Accurate experimental data are also needed to validate the various theoretical nuclear models [13]. In view of this, in the present work, cross sections for the $^{186}$W$(n,\gamma)^{187}$W, $^{183}$W$(n,p)^{183}$Ta, $^{154}$Gd$(n,2n)^{153}$Gd, and $^{160}$Gd$(n,2n)^{159}$Gd reactions at the neutron energies of $5.08 \pm 0.165$, $8.96 \pm 0.77$, $12.47 \pm 0.825$, and $16.63 \pm 0.95$ MeV were measured by neutron activation analysis (NAA) and the off-line $\gamma$ ray spectrometry technique. The above mentioned reaction cross sections were also calculated by using the computer codes TALYS 1.8 and EMPIRE 3.2.2. Different LD models available in TALYS 1.8 and Levden models in EMPIRE 3.2.2 were used to validate the present experimental results.

In this paper, the experimental details are discussed in Sec. II. Section III describes the data analysis. The neutron flux and average neutron energy calculations used to obtain reaction cross sections, with suitable corrections incorporated to obtain accurate cross section results, are also discussed in this section. Section IV presents the theoretical calculations, followed by results and discussions in Sec. V. A summary and conclusions are given in Sec. VI.

## II. EXPERIMENTAL DETAILS

The experiment was carried out by using the BARC-TIFR Pelletron facility in Mumbai, India. The neutrons were produced using the $^7$Li$(p,n)^7$Be reaction. A proton beam was targeted on natural lithium foil of thickness 8.0 mg/cm$^2$. The Li foil was wrapped with 3.7 mg/cm$^2$ tantalum in front and 4.12 mg/cm$^2$ on the back. The energies of the proton beam were selected to be 7.0, 11.0, 15.0, and 18.8 MeV. The samples were kept at a distance of 2.1 cm from the Li target in the

*Corresponding author: sk.mukherjee-phy@msubaroda.ac.in

TABLE I. Details of the irradiation in the present experiment.

|  | Irradiation 1 | Irradiation 2 | Irradiation 3 | Irradiation 4 |
|---|---|---|---|---|
| Proton energy (MeV) | 18.8 | 7.0 | 15.0 | 11.0 |
| Total irradiation time (h:min) | 5:00 | 11:15 | 7:00 | 16:05 |
| Beam current (nA) | 150 | 110 | 150 | 120 |

forward direction. The targets were irradiated for different irradiation times. The irradiation details are given in Table I. A schematic view of the irradiation setup is shown in Fig. 1. In the present measurements, the natural samples of W (99.97%) in the form of 1.0 mm thick and about a quarter of a circle with radius of 1 to 3 cm were used. Gd samples were made in the form of a pellet with radius of 0.65 cm and of thickness from 0.5 to 1.0 mm using $Gd_2O_3$ (99.9%) powder. The weight of the samples was measured using a digital microbalance weighing machine. The mass of W samples in different sets of irradiations were 3.6689 g (irradiation 1), 0.7826 g (irradiation 2), 0.8344 g (irradiation 3), and 0.504 g (irradiation 4). The samples of Gd were with mass of 0.4071 g (irradiation 1) and 0.9102 g (irradiation 3). In each irradiation, indium (In) and thorium (Th) foils were used as flux monitors. After a suitable cooling time, the irradiated samples were mounted on different Perspex plates and kept in front of the precalibrated high purity germanium (HPGe) detector. A Baltic company HPGe detector with 4-K channels MCA and MAESTRO spectroscopic software was used to measure the $\gamma$ ray spectra from the irradiated sample. The HPGe detector system was calibrated using a standard $^{152}Eu$ multi-$\gamma$-ray source. The efficiency of the detector was also determined at different $\gamma$ energies using the same source. The $\gamma$ ray activities of the irradiated samples were measured for different counting times. The prominent $\gamma$ ray energies emitted from the irradiated samples and other spectroscopic data are given in Table II. Isotopic abundances are taken from the literature [14]. The threshold energies of the reactions are calculated using the $Q$ value calculator provided online by National Nuclear Data Centre (NNDC) [15]. The daughter nuclide half-life and details of the emitted prominent $\gamma$ rays are taken from the literature [16]. Typical $\gamma$ ray spectra obtained from the irradiated W and Gd samples are shown in Figs. 2(a)–2(b).

## III. DATA ANALYSIS

### A. Neutron activation analysis

The experimental data were analyzed by using the standard neutron activation analysis (NAA) technique. In this technique,
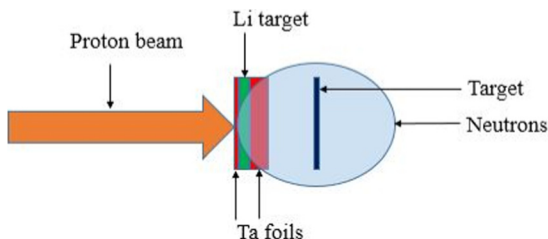


FIG. 1. Experimental arrangement showing neutron production using Li($p$,$n$) reaction.

the nuclear reaction rate or the rate of production of daughter isotopes depends on the number of target nuclei available and the neutron flux incident on it. This activation method is generally followed to measure reaction cross section by irradiating the target isotope with neutrons, when the products emit characteristic $\gamma$ rays having sufficiently long half-life and $\gamma$ branching abundances. The cross section of the selected reactions can be determined using the following equation [17]:

$$\sigma = \frac{A_\gamma \lambda (t_c/t_r)}{N \phi I_\gamma \varepsilon (1 - e^{-\lambda t_i})(1 - e^{-\lambda t_c}) e^{-\lambda t_w}}, \quad (1)$$

where

$A_\gamma$ = number of detected $\gamma$ ray counts;

$\lambda$ = decay constant of product nucleus ($s^{-1}$);

$t_i$ = irradiation time (s);

$t_w$ = cooling time (s);

$t_c$ = counting time (s);

$t_r$ = real time (clock time) (s);

$\phi$ = incident neutron flux ($n\,cm^{-2}\,s^{-1}$);

$I_\gamma$ = branching intensity of $\gamma$ ray;

$\varepsilon$ = efficiency of detector for the chosen $\gamma$ ray;

$N$ = number of target atoms.

In the above equation, the activity ($A_\gamma$) is measured using an HPGe detector for different $\gamma$ rays emitted from the daughter isotopes. Because of the half-lives of the isotopes of interest, several rounds of $\gamma$ ray counting were done. The dead time of the detector system was kept below 0.6% during the entire counting process. The numbers of target nuclei were calculated from the weight of the sample and isotopic abundances. The calculation of the neutron flux was done using the $\gamma$ ray spectra of irradiated In and Th foils. Other standard parameters of the reactions were taken from the literature [14–16].

### B. Neutron flux and average neutron energy

The neutrons were generated by $^7Li(p,n)^7Be$ reactions. Below 2.4 MeV, this reaction produces monoenergetic neutrons [18]. Above 2.4 MeV, the first excited state of $^7Be$ at 0.43 MeV is populated and produces a second group of neutrons [18,19]. Above 6 MeV, the three body interaction and other excited states also contribute in the neutron production along with the main neutron group [18,19]. Although there are lower energy subgroups of neutrons, the primary (main) group of neutrons can be used to measure the reaction cross section as it has higher neutron flux and higher neutron energy (forming a peak). The reaction cross section measured at this

TABLE II. Selected nuclear reactions, target isotopic abundance, threshold energy of reaction, product nucleus with half-life, and energies of prominent $\gamma$ rays with branching intensities.

| Reaction | Isotopic abundance (%) [14] | Threshold energy (MeV) [15] | Product nucleus | Half-life [16] | Prominent $\gamma$-ray energy (keV); (branching intensity %) [16] |
|---|---|---|---|---|---|
| $^{186}$W$(n,\gamma)^{187}$W | 28.43 | | $^{187}$W | 24.0 h | 479.5(26.6); 685.7(33.2) |
| $^{182}$W$(n,p)^{182}$Ta | 26.50 | 1.037 | $^{182}$Ta | 114.74 d | 1121.3(35.24) |
| $^{154}$Gd$(n,2n)^{153}$Gd | 2.18 | 8.953 | $^{153}$Gd | 240.4 d | 103.1(21.1) |
| $^{160}$Gd$(n,2n)^{159}$Gd | 21.86 | 7.498 | $^{159}$Gd | 18.479 h | 363.5(11.78) |

averaged peak energy. The spectrum averaged neutron energy can be given as [20]

$$E_{\mathrm{mean}} = \frac{\int_{E_{\mathrm{ps}}}^{E_{\mathrm{max}}} E_i \phi_i \, dE}{\int_{E_{\mathrm{ps}}}^{E_{\mathrm{max}}} \phi_i \, dE}, \tag{2}$$
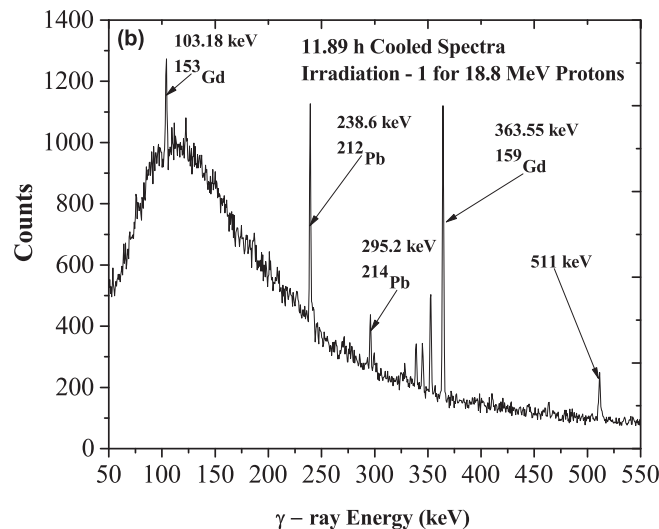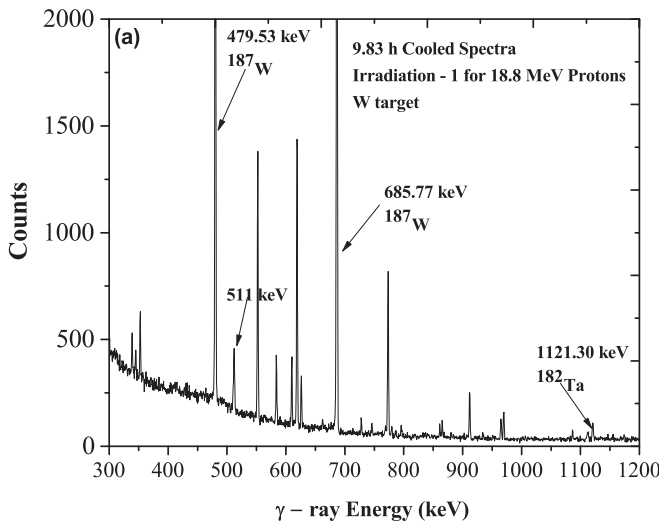


where

$E_{\mathrm{ps}}$ = peak forming start neutron energy;

$E_{\mathrm{max}}$ = maximum neutron energy;

$E_i$ = energy bin;

$\phi_i$ = neutron flux of energy bin $E_i$;

$E_{\mathrm{mean}}$ = effective mean energy.

The neutron spectra for 7.0, 11.0, 15.0, and 18.8 MeV were derived by taking data from various available publications [18–22]. The neutron spectra corresponding to all the four incident proton energies are shown in Figs. 3(a)–3(d). The average peak energies obtained by using Eq. (2) are given in Table III.

In order to analyze the data, it is necessary to accurately calculate the neutron flux incident on the target. In the present experiment, $^{115}$In$(n,n')^{115m}$In and $^{232}$Th$(n,f)^{97}$Zr monitor reactions were used for the neutron flux measurement. The reaction products $^{115m}$In and $^{97}$Zr have a half-life of 4.486 and 16.749 h respectively [16]. The emitted characteristic $\gamma$ lines are given in Table IV. Typical $\gamma$ ray spectra obtained from both the monitors are shown in Fig. 4.

The calculations of the neutron flux incident on the target were done by using the spectrum averaged neutron cross section for the monitor reactions by using the relatively recent data available from the EXFOR data library for $^{115}$In$(n,n')$ [23–26] and for $^{232}$Th$(n,f)$ [27–30]. The spectrum averaged cross section was calculated using the following equation:

$$\sigma_{\mathrm{av}} = \frac{\int_{E_{th}}^{E_{\mathrm{max}}} \sigma_i \phi_i \, dE}{\int_{E_{\mathrm{th}}}^{E_{\mathrm{max}}} \phi_i \, dE}, \tag{3}$$

where

$E_{\mathrm{th}}$ = threshold energy of the monitor reaction;

$E_{\mathrm{max}}$ = maximum neutron energy;

$\sigma_i$ = cross section at energy $E_i$ for monitor reaction from EXFOR [23–30];

$\phi_i$ = neutron flux of energy bin $E_i$ from the Figs. 5(a)–5(d);

$\sigma_{\mathrm{av}}$ = spectrum averaged cross section.

The calculated spectrum averaged cross sections for both the monitor reactions are given in Table III. The neutron flux incident on targets for all the four irradiations were calculated

FIG. 2. (a) Typical $\gamma$ ray spectra for W target obtained by using HPGe detector. (b) Typical $\gamma$ ray spectra for Gd target obtained by using HPGe detector.
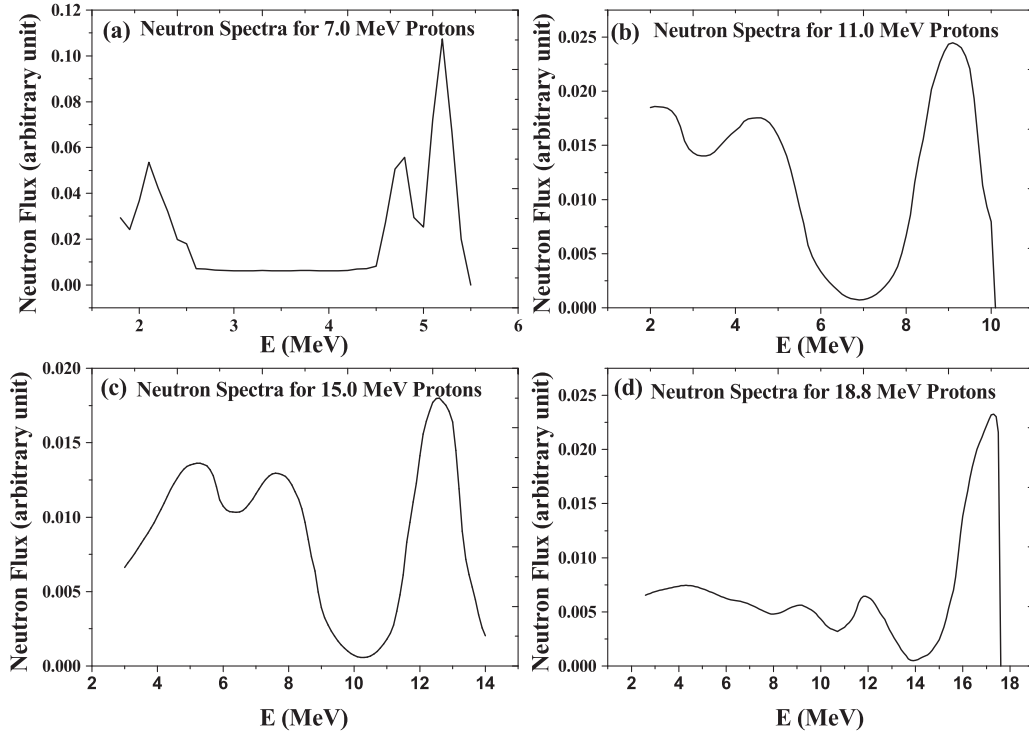
FIG. 3. (a)–(d) $^7$Li$(p,n)^7$Be neutron spectra for the 7.0 (a), 11.0 (b), 15.0 (c), and 18.8 (d) MeV proton energies.

using the following activation equation:

$$\phi = \frac{A_\gamma \lambda (t_c/t_r)}{N \sigma_{av} I_\gamma \varepsilon (1 - e^{-\lambda t_i})(1 - e^{-\lambda t_c}) e^{-\lambda t_w}}. \qquad (4)$$

All the parameters are same as in Eq. (1).

In the case of a fission reaction monitor, the fission yield term ($Y$) will come in the denominator on the right side of the above Eq. (4). In the cross section calculations, the measured values of the average neutron flux from both the monitors were taken, as both these values are in agreement with each other within the limits of the experimental errors as discussed later in Sec. V.

### C. Cross section correction for lower energy neutrons

In order to measure the cross section for neutrons of main peak, it is necessary to make corrections due to the contributions from lower energy neutrons. This correction is not required when the neutron source is purely monoenergetic, which is not the present case. As mentioned earlier, in addition to a primary neutron group, there exist secondary neutron groups arising due to an excited state of $^7$Be and three-body reactions above 2.4 and 6 MeV respectively [18]. These secondary groups produce neutrons at lower energies and in addition to the primary group neutrons [18,19]. As the primary neutron exhibits a distinct broad peak always at much higher energy with a high neutron flux, it can be considered as a quasimonoenergetic source. It is possible to remove the contributions to the reaction cross sections due to

TABLE III. The spectrum averaged neutron energies and respective neutron flux from two different monitor reactions.

| | Irradiation 1 | Irradiation 2 | Irradiation 3 | Irradiation 4 |
|---|---|---|---|---|
| Proton energy (MeV) | 18.8 | 7.0 | 15.0 | 11.0 |
| Neutron energy from Eq. (2) (MeV) | $16.63 \pm 0.95$ | $5.08 \pm 0.165$ | $12.47 \pm 0.825$ | $8.96 \pm 0.77$ |
| Spectrum averaged cross section for In monitor (mb) | 188.94 | 223.88 | 253.79 | 302.85 |
| Calculated neutron flux from $^{115}$In$(n,n')^{115m}$In $(n\,cm^{-2}\,s^{-1})$ | $6.2891 \times 10^7$ | $4.6304 \times 10^6$ | $1.8054 \times 10^7$ | $1.6009 \times 10^6$ |
| Spectrum averaged cross section for Th monitor (mb) | 341.67 | 99.04 | 269.58 | 220.01 |
| Calculated neutron flux from $^{232}$Th$(n,f)^{97}$Zr $(n\,cm^{-2}\,s^{-1})$ | $6.2885 \times 10^7$ | $4.5709 \times 10^6$ | $1.7090 \times 10^7$ | $1.5850 \times 10^6$ |

TABLE IV. The monitor reaction with the product nucleus and prominent $\gamma$ lines.

| Monitor reaction | Product nucleus (half-life) [16] | Prominent $\gamma$ line (branching intensity %) [16] |
|---|---|---|
| $^{115}$In$(n,n')^{115m}$In | $^{115m}$In (4.486 h) | 336.24 (45.8) |
| $^{232}$Th$(n,f)^{97}$Zr | $^{97}$Zr (16.749 h) | 743.36 (93.0) |

low energy neutrons from the primary neutron group by the process of making a tailing correction. In the present work, the tailing correction has been done using the method given in the literature [20].

The cross sections have been calculated using the NAA Eq. (1) and the neutron flux from monitor reactions. For a capture reaction, one has to use total neutron flux, but for the reactions having threshold energy, the neutron flux must be corrected. To do this, one has to remove the neutron flux from minimum to threshold energy neutrons, by taking the area under the neutron spectra. For instance, the $^{154}$Gd$(n,2n)^{153}$Gd reaction has a threshold energy of 8.953 MeV. Hence, the flux for this reaction must be the area under the curve shown from "**A**" (threshold energy) to "**B**" (maximum neutron energy) (Fig. 5). This will correct the actual neutron flux used to produce the desired daughter isotopes. Using this neutron flux, a set of cross sections of all reactions has been calculated. In order to remove the effective spectrum average cross section from the threshold to the minimum energy of the peak of interest ($E_{ps}$), theoretical calculations using modular code TALYS 1.8 have been carried out to obtain the reaction cross sections versus neutron energy. These calculated cross sections at different energies are convoluted with the neutron flux as shown in Fig. 3(a). The spectrum average cross section for each reaction was calculated from threshold to minimum energy ($E_{ps}$), and it is subtracted from the previous cross section dataset. Thus the final value obtained gives the cross section for the reaction at the spectrum average neutron peak energy.

Using the above method, the cross sections for the $^{182}$W$(n,p)^{182}$Ta, $^{186}$W$(n,\gamma)^{187}$W, $^{154}$Gd$(n,2n)^{153}$Gd, and $^{160}$Gd$(n,2n)^{159}$Gd reactions were measured at the neutron

energies of 5.08, 8.96, 12.47, and 16.63 MeV. In the $^{160}$Gd$(n,2n)^{159}$Gd and $^{158}$Gd$(n,\gamma)^{159}$Gd reactions, a common $\gamma$ ray of 363.54 keV ($I\gamma = 11.78\%$) is emitted. Therefore, it is necessary to remove this part of the cross section from this capture reaction. At higher energies, the $(n,\gamma)$ reaction has a very small contribution compared to the lower energy neutrons. Since the lower energy neutron part has been already corrected using the above method, the cross section obtained is purely due to the $(n,2n)$ reaction. In the same way, the tailing corrections have been applied for all the reactions studied in the present work.

## IV. THEORETICAL CALCULATIONS

In order to theoretically understand the measured cross section results, two well-known nuclear reaction modular codes, TALYS 1.8 and EMPIRE 3.2.2, were used [13]. Both codes are being used worldwide for nuclear data prediction for the emission of $\gamma$, neutron, proton, deuteron, triton, and other particles. Both codes used the reaction parameters from the RIPL database [31]. These codes consider the effect of level density parameters, compound, pre-equilibrium, and direct reaction mechanisms as a function of incident particle energy. The optical model parameters were obtained by using a global potential, proposed by Koning and Delaroche [32]. The compound reaction mechanism was incorporated using the Hauser-Feshbach model [33]. The pre-equilibrium contribution was accounted for by an exciton model that was developed by Kalbach [34]. In the present work, the



FIG. 4. Typical monitor reaction $\gamma$ ray spectra using HPGe detector.
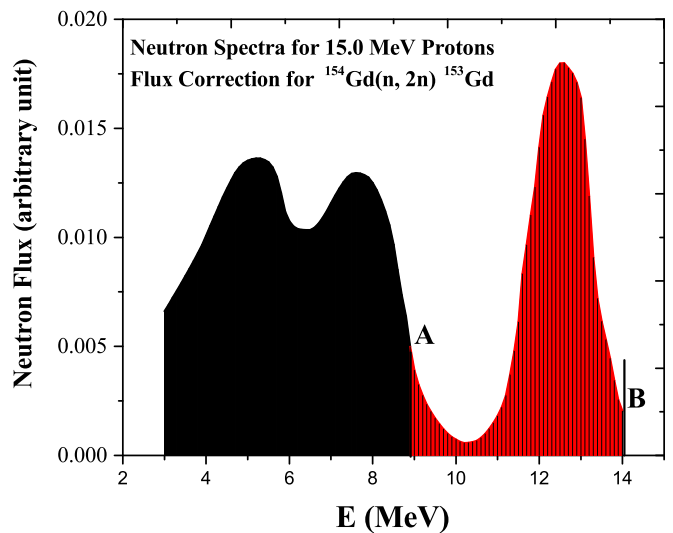


FIG. 5. Neutron flux correction for the threshold energy reactions, shown for $^{154}$Gd$(n,2n)^{153}$Gd reaction with threshold energy of 8.953 MeV labeled by **A** and maximum neutron energy labeled by **B**.
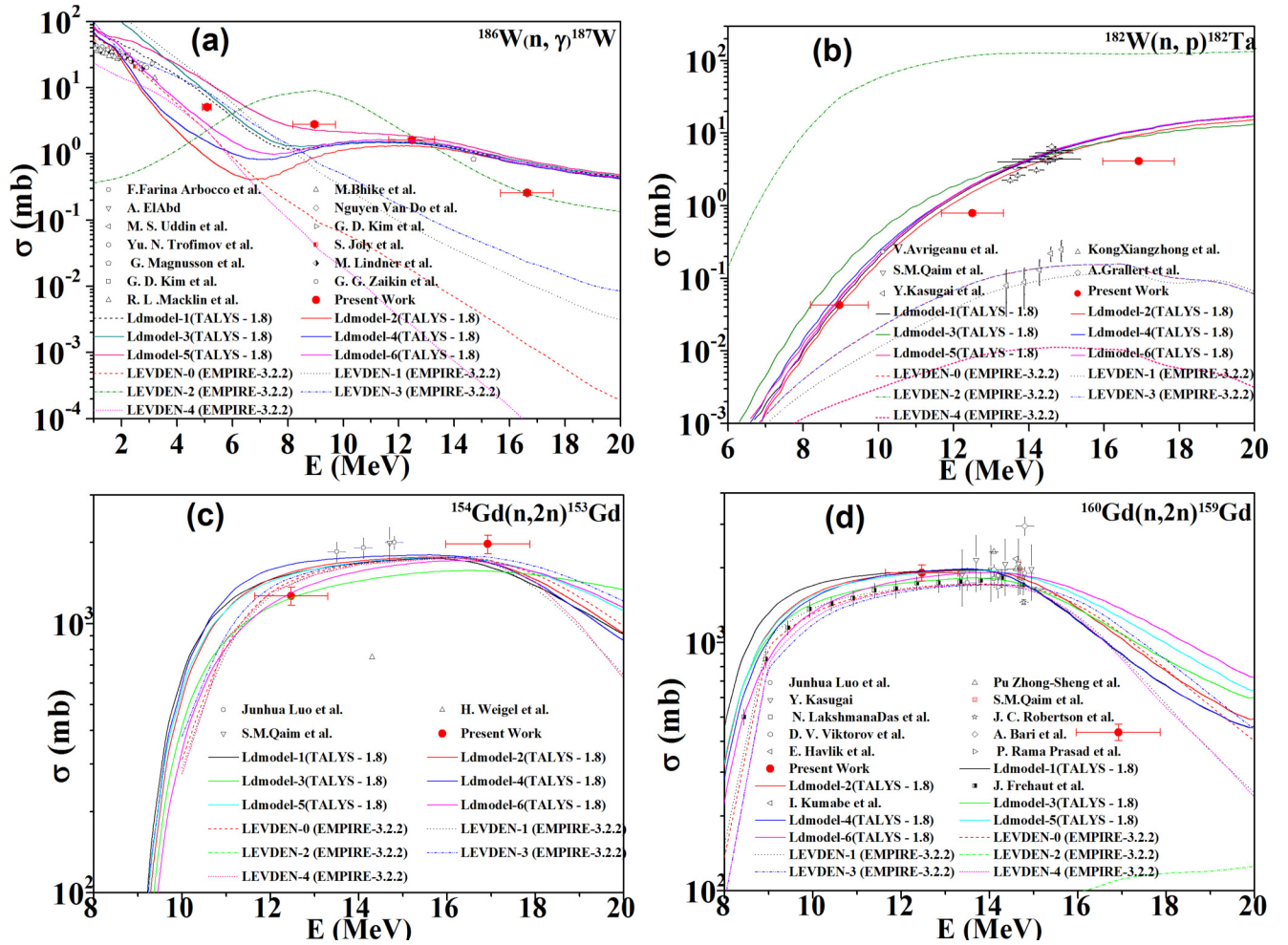
FIG. 6. (a)–(d) Present measured cross section for $^{186}$W$(n,\gamma)^{187}$W and $^{182}$W$(n,p)^{182}$Ta, $^{154}$Gd$(n,2n)^{153}$Gd and $^{160}$Gd$(n,2n)^{159}$Gd reactions compared with EXFOR and predicted cross section data using different theoretical nuclear models of TALYS 1.8 and EMPIRE 3.2.2; The LEVDE-2 model of EMPIRE 3.2.2 predicts very low values (below 100 mb) of cross sections comparing to other models hence it cannot be seen in plot of $^{154}$Gd$(n,2n)^{153}$Gd.

calculations have been done with all the default parameters except changing the LD model and level density parameters. The present results along with EXFOR data were compared with these predicted data as shown in Figs. 6(a) and 6(b).

## V. RESULTS AND DISCUSSION

The main objective of the present study was to provide a set of reaction cross section data in the energy range where there are very few or no measurements available in the literature. These cross sections are important for the accurate reactor design and also to improve the existing nuclear database. Hence the present experimental data for W and Gd isotopes become more important. Further, in this energy region, the standard nuclear models play an important role to validate the present measured experimental data. The major uncertainties in the present reaction cross sections are given in Table V.

The measured data were supported by the theoretical predictions using EMPIRE 3.2.2 and TALYS 1.8. There are different options of level density given in EMPIRE 3.2.2. The level density parameter values Levden = 0, 1, 2, 3, 4 uses

various well known models described in various publications [31,35–39]. By varying these parameters, the cross section for the selected reactions from threshold to 20 MeV were calculated. The predicted and experimental results are shown in Figs. 6(a)–6(d). In TALYS 1.8, the different LD model options were varied from LD model 1 to LD model 6 for the selected nuclear reactions and the experimental cross sections

TABLE V. Major uncertainties incorporated in the present cross section results.

| Parameter | Limit (%) |
|---|---|
| Counting rate | $\leqslant$4–5 |
| Efficiency calibration | $\leqslant$3 |
| Self-absorption | $\leqslant$0.2 |
| Mass | $\leqslant$0.001 |
| Neutron flux | $\leqslant$6 |
| $I_\gamma$ | $\leqslant$3 |

TABLE VI. Comparison of present experimental data different model predictions using TALYS 1.8 and EMPIRE 3.2.2.

| Energy (MeV) | Measured | TALYS 1.8 | | | | | | EMPIRE 3.2.2 | | | | |
|---|---|---|---|---|---|---|---|---|---|---|---|---|
| | | LD model 1 | LD model 2 | LD model 3 | LD model 4 | LD model 5 | LD model 6 | Levden 0 | Levden 1 | Levden 2 | Levden 3 | Levden 4 |

$^{186}$W$(n,\gamma)^{187}$W reaction cross section (mb)

| Energy (MeV) | Measured | LD model 1 | LD model 2 | LD model 3 | LD model 4 | LD model 5 | LD model 6 | Levden 0 | Levden 1 | Levden 2 | Levden 3 | Levden 4 |
|---|---|---|---|---|---|---|---|---|---|---|---|---|
| 5.08 ± 0.165 | 5.079 ± 0.39 | 7.23 | 0.885 | 8.37 | 1.53 | 12.1 | 2.80 | 2.24 | 12.8 | 2.24 | 8.83 | 2.2903 |
| 8.96 ± 0.77 | 2.767 ± 0.19 | 1.22 | 0.871 | 1.31 | 1.17 | 2.26 | 1.26 | 0.108 | 0.618 | 9.01 | 0.827 | 0.0453 |
| 12.47 ± 0.825 | 1.620 ± 0.11 | 1.46 | 1.30 | 1.48 | 1.43 | 1.81 | 1.58 | 0.0181 | 0.0794 | 1.86 | 0.146 | 0.0027 |
| 16.63 ± 0.95 | 0.257 ± 0.02 | 0.726 | 0.676 | 0.753 | 0.683 | 0.799 | 0.716 | 0.00129 | 0.0107 | 0.249 | 0.0226 | 8.41E-5 |

$^{182}$W$(n,p)^{182}$Ta reaction cross section (mb)

| Energy (MeV) | Measured | LD model 1 | LD model 2 | LD model 3 | LD model 4 | LD model 5 | LD model 6 | Levden 0 | Levden 1 | Levden 2 | Levden 3 | Levden 4 |
|---|---|---|---|---|---|---|---|---|---|---|---|---|
| 8.96 ± 0.77 | 0.043 ± 0.003 | 0.04813 | 0.04141 | 0.12659 | 0.06359 | 0.05509 | 0.05307 | 0.00964 | 0.00544 | 31.0747 | 0.00964 | 0.00194 |
| 12.47 ± 0.825 | 0.793 ± 0.06 | 1.789 | 1.52 | 2.33301 | 1.87 | 1.86 | 1.92 | 0.0842 | 0.0495 | 118 | 0.0842 | 0.00803 |
| 16.63 ± 0.95 | 4.092 ± 0.28 | 10.2 | 8.89 | 8.4404 | 10.2 | 10.4 | 10.5 | 0.163 | 0.147 | 124 | 0.163 | 0.0107 |

$^{154}$Gd$(n,2n)^{153}$Gd cross section (mb)

| Energy (MeV) | Measured | LD model 1 | LD model 2 | LD model 3 | LD model 4 | LD model 5 | LD model 6 | Levden 0 | Levden 1 | Levden 2 | Levden 3 | Levden 4 |
|---|---|---|---|---|---|---|---|---|---|---|---|---|
| 12.47 ± 0.825 | 1265 ± 98 | 1534 | 1556 | 1248 | 1659 | 1520 | 1298 | 1444 | 1412 | 22.2 | 1479 | 1397 |
| 16.63 ± 0.95 | 1973 ± 153 | 1683 | 1725 | 1571 | 1737 | 1735 | 1703 | 1748 | 1744 | 65.3 | 1774 | 1744 |

$^{160}$Gd$(n,2n)^{159}$Gd cross section (mb)

| Energy (MeV) | Measured | LD model 1 | LD model 2 | LD model 3 | LD model 4 | LD model 5 | LD model 6 | Levden 0 | Levden 1 | Levden 2 | Levden 3 | Levden 4 |
|---|---|---|---|---|---|---|---|---|---|---|---|---|
| 12.47 ± 0.825 | 1913 ± 143 | 1938 | 1919 | 1765 | 1935 | 1901 | 1828 | 1669 | 1679 | 52.9 | 1642 | 1660 |
| 16.63 ± 0.95 | 435 ± 33 | 1009 | 1155 | 1183 | 1005 | 1364 | 1465 | 1213 | 1027 | 106 | 1282 | 999 |

were compared. The details of these parameters are given in the TALYS 1.8 manual [39,40].

As shown in Fig. 6(a) for the $^{186}$W$(n,\gamma)^{187}$W reaction, the Levden = 2 of EMPIRE 3.2.2 gives a relatively better agreement compared to other Levden values. But at lower energy the Levden = 2 does not give satisfactory predictions. Moreover, all other level density models of EMPIRE 3.2.2 show discrepancies with each other and predicts a lower cross section as compared to the present experimental results. In the case of TALYS 1.8 analyses, results of all the LD model options are in good agreement with the data of present measurements. For the $^{182}$W$(n,p)^{182}$Ta reaction, all TALYS 1.8 LD model are in good agreement. The EMPIRE Levden models show a discrepancy with most of EXFOR and the present data. For the $^{154}$Gd$(n,2n)^{153}$Gd and $^{160}$Gd$(n,2n)^{159}$Gd reactions, the experimental results are in good agreement with both the TALYS 1.8 and EMPIRE 3.2.2 predictions, except Levden = 2, being listed as a future option in the EMPIRE input file. Only the measurement at 16.63 MeV neutron energy of $^{160}$Gd$(n,2n)^{159}$Gd is under estimated then the predicted values. Overall the theoretical predictions support the present results. The measured cross section values and the different model predicted values are compared at the same energies in Table VI. In general, TALYS 1.8, for all the selected models, gives better agreement compared to EMPIRE 3.2.2 in predicting the present experimental results.

## VI. SUMMARY AND CONCLUSIONS

Cross sections for the $^{182}$W$(n,p)^{182}$Ta, $^{186}$W$(n,\gamma)^{187}$W, $^{154}$Gd$(n,2n)^{153}$Gd, and $^{160}$Gd$(n,2n)^{159}$Gd reactions were measured at the neutron energies $5.08 \pm 0.165$, $8.96 \pm 0.77$, $12.47 \pm 0.825$, and $16.63 \pm 0.95$ MeV by using the neutron activation analysis technique and incorporating standard tailing corrections [18]. The cross sections have been measured in an energy range where very few or no measurements are available. The different correction terms are discussed in order to

achieve accurate cross section results. The spectrum averaged neutron energy and accurate flux measurements have also been duly incorporated. The neutron flux at different energies has been calculated by using two monitor reactions and the values thus obtained were found to be in good agreement. The average flux values from the two monitor reactions were taken for cross sections calculation. The cross sections for the $^{186}$W$(n,\gamma)^{187}$W reaction have been measured at four different energies. In the case of $^{182}$W$(n,p)^{182}$Ta the cross sections are reported at $8.96 \pm 0.77$, $12.47 \pm 0.825$, and $16.63 \pm 0.95$ MeV. For the $^{154}$Gd$(n,2n)^{153}$Gd and $^{160}$Gd$(n,2n)^{59}$Gd reactions, the cross sections are reported at $12.47 \pm 0.825$, and $16.63 \pm 0.95$ MeV neutron energies. All the measurements have been compared with the theoretical modular codes TALYS 1.8 and EMPIRE 3.2.2. It may be concluded that TALYS 1.8 gives an overall satisfactory agreement with the present experimental and EXFOR results for most of the selected LD model as compared to EMPIRE 3.2.2 predictions. However, in the case of $(n,\gamma)$ reaction, Levden = 2 of EMPIRE gives somewhat better predictions as compared to other Levden models in the energy region above 12 MeV. The cross section data presented in this work are important for the future fission/fusion reactor technology.

[1] A. J. Koning and J. Blomgren, Nuclear data for sustainable nuclear energy, JRC Scientific and Technical Report No. EUR23977EN-2009, 2009, retrieved from https://cordis.europa.eu/pub/fp6-euratom/docs/candide-final-report_en.pdf.

[2] Cross Section Information Storage and Retrieval System (EXFOR), IAEA, Vienna, Austria, http://www.nds.iaea.or.at/exfor/ (online).

[3] M. Lehnen *et al.*, J. Nucl. Mater. **463**, 39 (2015).

[4] J. Qing, Y. Wu, M. Regis, and J. W. Kwan, IEEE Trans. Nucl. Sci. **56**, 1312 (2009).

[5] J. Reijonen, F. Gicquel, S. K. Hahto, M. King, T. P. Lou, and K. N. Leung, Appl. Radiat. Isotopes **63**, 757 (2005).

[6] Y. Wu, J. P. Hurley, Q. Ji, J. Kwan, and K. N. Leung, IEEE Trans. Nucl. Sci. **56**, 1306 (2009).

[7] V. Voitsenya *et al.*, Rev. Sci. Instrum. **72**, 475 (2001).

[8] G. De Temmerman, R. A. Pitts, V. S. Voitsenya, L. Marot, G. Veres, M. Maurer, and P. Oelhafen, J. Nucl. Mater. **363-365**, 259 (2007).

[9] K. H. Behringer, J. Nucl. Mater. **145**, 145 (1987).

[10] Y. Gohar, I. Bolshinsky, and I. Karnaukhov, NEA/NSC/DOC(2015)7, 254(2015), retrieved from http://www.oecd.org/officialdocuments/publicdisplaydocumentpdf/?cote=NEA/NSC/DOC(2015)7&docLanguage=En.

[11] R. Vijayalakshmi, D. K. Singh, M. K. Kotekar, and H. Singh, J. Radioanal. Nucl. Chem. **300**, 129 (2014)

[12] S. Dutta, P. Suryanarayanan, A. R. Kandalgaonkar, R. S. Sharma, H. Bose, and V. K. P. Unny, BARC News Lett. **271**, 2 (2006).

[13] N. Dzysiuk, I. Kadenko, A. J. Koning, and R. Yermolenko, Phys. Rev. C **81**, 014610 (2010).

[14] K. J. R. Rosman and P. D. P. Taylor, Pure Appl. Chem. **70**, 217 (1998).

[15] http://www.nndc.bnl.gov/qcalc/index.jsp, retrieved on 11 November 2016.

[16] http://www.nndc.bnl.gov/nudat2/indx_dec.jsp, retrieved on 21 March 2017.

[17] V. Vansola *et al.*, Radiochim. Acta **103**, 817 (2015).

[18] C. H. Poppe, J. D. Anderson, J. C. Davis, S. M. Grimes, and C. Wong, Phys. Rev. C **14**, 438 (1976).

[19] J. D. Anderson, C. Wong, and V. A. Madsen, Phys. Rev. Lett. **24**, 1074 (1970).

[20] D. L. Smith *et al.*, Corrections for Low Energy Neutrons by Spectral Indexing, retrieved from https://www.oecdnea.org/science/docs/2005/nsc-wpec-doc2005-357.pdf.

[21] P. M. Prajapati *et al.*, Eur. Phys. J. A **48**, 1 (2012).

[22] M. W. Mcnaughton, N. S. P. King, F. P. Brady, J. L. Romero, and T. S. Subramanian, Nucl. Instrum. Methods **130**, 555 (1975).

[23] A. A. Lapenas, *Neutron* (ZINATNE, Riga, USSR, 1975), p. 80.

[24] G. Loevestam, M. Hult, A. Fessler, T. Gamboni, J. Gasparro, R. Jaime, P. Lindahl, S. Oberstedt, and H. Tagziria, Nucl. Instrum. Methods Phys. Res., Sect. A **580**, 1400 (2007).

[25] Y. Agus, I. Celenk, and A.Ozmen, Radiochim. Acta **92**, 63 (2004).

[26] M. S. Uddin, S. Sudar, S. M. Hossain, R. Khan, M. A. Zulquarnain, and S. M. Qaim, Radiochim. Acta **101**, 613 (2013).

[27] O. A. Shcherbakov, A. Yu. Donets, A. V. Evdokimov *et al.*, in *International Seminar on Interactions of Neutrons with Nuclei, Dubna, Russia, 2001* (2001), Vol. 9, p. 257.

[28] R. K. Jain, Pramana **49**, 515 (1997).

[29] I. Garlea, Chr. Miron-Garlea, H.N. Rosu, G. Fodor, and V. Raducu, Rev. Roum. Phys. **37**, 19 (1992).

[30] F. Manabe, K. Kanda, T. Iwasaki, H. Terayama, Y. Karino, M. Baba, and N. Hirakawa, Fac. of Engineering, Tohoku Univ. Tech. Report 52(Issue 2) (1988) 97.

[31] R. Capote *et al.*, Nucl. Data Sheets **110**, 3107 (2009).

[32] A. J. Koning and J. P. Declaroche, Nucl. Phys. A **713**, 231 (2003).

[33] W. Hauser and H. Feshbach, Phys. Rev. **87**, 366 (1952).

[34] C. Kalbach, Phys. Rev. C **33**, 818 (1986).

[35] https://www-nds.iaea.org/RIPL-3/densities/, retrieved on 28 February 2017.

[36] A. V. Ignatyuk, K. K. Istekov, and G. N. Smirenkin, Sov. J. Nucl. Phys. **29**, 450 (1979).

[37] A. V. Ignatyuk, J. L. Weil, S. Raman, and S. Kahane, Phys. Rev. C **47**, 1504 (1993).

[38] A. Gilbert and A. G. W. Cameron, Can. J. Phys. **43**, 1446 (1965).

[39] S. Hilaire, M. Girod, S. Goriely, and A. J. Koning, Phys. Rev. C **86**, 064317 (2012).

[40] A. Koning, S. Hilaire, and S. Goriely, *TALYS-1.6 - A Nuclear Reaction Program*, User Manual, 1st ed. (NRG, Westerduinweg, 2013).